Final Technical Report

Project title: Materials for Ultra-Coherent, Mobile, Electron-Spin Qubits

Award number: DE-SC0020136

DOE Office of Basic Energy Sciences

Project period: 09/15/2019 - 09/14/2023

Organization (prime): Princeton University

Principal Investigator:
Stephen A. Lyon
Department of Electrical and Computer Engineer
Princeton University
EQuad
Princeton, NJ 08544

Co-Principal Investigator:
Mark Dykman
Department of Physics and Astronomy
Michigan State University
Biomedical Physical Sciences Bldg.
567 Wilson Road, Room 4244
East Lansing, MI 48824-2320

Separately funded Co-investigators/collaborators
Eric Shaner and
M. David Henry
Luke A. D'Imperio
Sandia National Laboratories
P.O. Box 5800
Albuquerque, NM 87185

Acknowledgement
We acknowledge financial support by the US Department of Energy under Contract Number DE-SC0020136

Sponsoring Program Office: Matthias Graf
Basic Energy Science
Office of Science
SC-32.2
US Department of Energy

Final Report

Stephen Lyon, Princeton University, Mark Dykman, Michigan State University

Eric Shaner, M. David Henry, and Luke D'Imperio, Sandia National Lab

The major goal of this project has been to better understand the physics of electrons bound to superfluid helium, especially electrons bound to thin helium films. An important aim has been to understand the spin properties of these electrons, since long spin coherence is crucial to the use of these electrons as mobile spin qubits. Through this project we have developed theories of spin coherence for both free 2-dimensional (2D) electrons and electrons bound in lithographically-defined quantum dots. We have extended the quantum dot calculation to calculations of spin manipulation using an applied magnetic field gradient of modest magnitude coupled with electric fields.

In the course of this work we have discovered other exciting new research directions and phenomena. As an outgrowth of experiments designed to increase the signal level for spin experiments, we demonstrated exceptionally high and stable electron densities above ultra-smooth amorphous metal films. These electrons are very likely Fermi degenerate, which will be the first time that a degenerate 2D electron gas has been conclusively demonstrated on helium. This work is continuing under other funding, and future publications will appropriately acknowledge the contributions of this grant. We have also investigated electron transport under unique conditions, including transport in a periodically modulated potential and high-mobility transport on thin van der Waals helium films. In addition a theory of many-body effects on intersubband transitions in this system has been published. New directions of this theory have been identified, including those that directly affect quantum information processing with electrons on helium and beyond, in particular, new approaches to controlling qubits based on defects in solids, including NV centers.

Here we will describe the results in more detail.

Spin Coherence

There has been both a theoretical and experimental component to the study of electron spin coherence. Previously, only very rough estimates have existed for the longitudinal (T_1) and transverse (T_2) spin relaxation times of electrons bound to He. We have considered both free 2D electrons as well as electrons bound in lithographically-defined lateral quantum dots.

For free electrons we have calculated the Rashba spin-orbit term, which dominates the spin relaxation at heterointerfaces in many semiconductor-based devices, Si-based structures in particular. At the helium-vacuum interface we find that this term is negligible, leading to relaxation times of the order of years. However, we have considered other terms associated with image-charge effects, and which are typically ignored in other systems where spin-orbit effects are much larger. We find that these image-charge effects dominate the spin relaxation, but still lead to extremely long spin coherence (hours for mobile electrons).

For electrons bound in quantum dots we have considered the combined effect on T_1 of excitation of an electron to a higher orbital state with ripplon scattering making up the energy difference between the spin-flip energy and the orbital excitation. In the absence of a spin-orbit interaction term, as occurs for electron in immobile single quantum states, there is no decoherence for an electron in a small quantum dot (dot with diameters less than about 1 μm at mK temperatures). This is analogous to Si-based quantum dots and donor impurities, where we have measured spin coherence of over 10 s, while free 2D electrons have a spin coherence of order 1 μs. However, by tuning the Larmor frequency close to the orbital excitation and applying an external magnetic field gradient it is possible to construct single qubit spin gates driven by a moderate microwave electric field. In this situation the ripplon scattering must be considered in detail. Together with the field gradient, the ripplons induce decoherence, but we have shown that high-fidelity gate operations can be performed with moderate microwave electric fields. We have also shown that the field gradient enables 2-qubit gates between electrons in neighboring dots, mediated by their electrostatic repulsion. The gate speeds are sufficient to achieve fidelity of 99.9%, in spite of decoherence allowed by the field gradient. This work has been published [1].

The calculation of the Rashba spin-orbit interaction for electrons bound to helium is not yet published, but a manuscript is in preparation. As noted earlier, this term in the spin orbit interaction dominates the spin relaxation and decoherence of free 2D electrons in Si-based heterostructures (Si/SiGe and Si/SiO_2), and it has been important to quantitatively analyze the helium-vacuum interface. For the case of an electron in a vacuum at the surface of superfluid helium we approximate the interface by assuming that the He is a crystalline solid, which allows us to calculate a band structure and the parameters needed to determine the magnitude of the effective Rashba field. In the absence of a strong external field pulling the electron against the surface (z-directed force), the electron is located about 7.6.nm above the He surface [2]. This is over an order of magnitude larger than the interatomic distance in the He, and thus the details of the atomic arrangement are expected to be averaged out. We will find that the Rashba term has such a small magnitude that a more exact

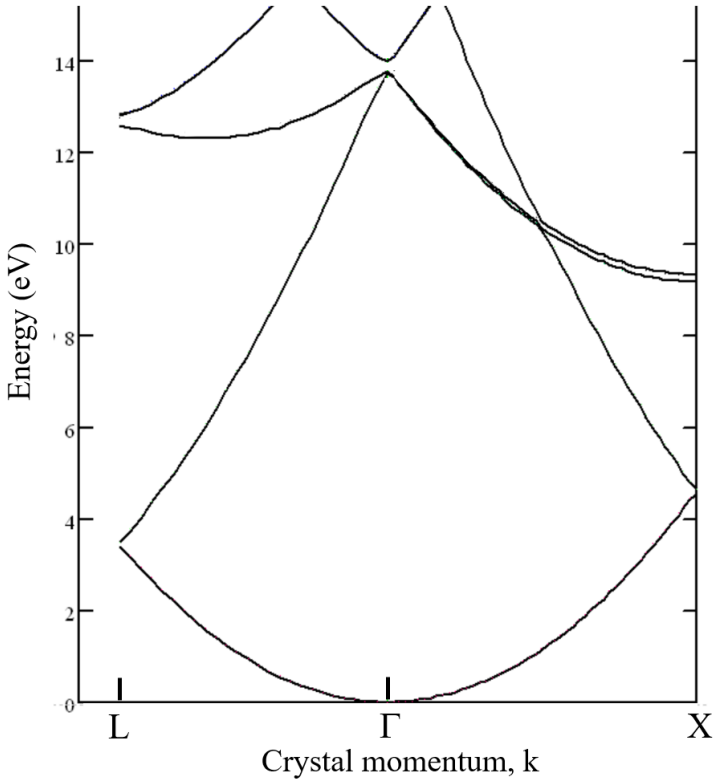

Figure 1. Calculated band structure for a helium crystal using the pseudopotentials from ref. []. An fcc crystal lattice with one atom/unit cell was assumed with a lattice constant of 0.568 nm to fit the atomic density of superfluid helium.

calculation does not appear to be warranted. We take the atomic arrangement of the solid He to be face-centered cubic, since that is a close-packed structure and the cubic symmetry simplifies the calculations. The lattice constant of this "pseudo-crystal" is chosen to match the atomic density of superfluid He.

The band structure calculation utilizes pseudopotentials for the helium. Several groups have published pseudopotential parameters for He atoms [3–5]. After testing these different parameter sets, we have found that those developed by Rama Krishna and Whaley for calculating the binding of electrons to He clusters to be the most suitable [3]. They were developed by fitting to s-wave and p-wave electron scattering phase shifts. Local pseudopotentials without a p-wave component give longer spin relaxation times. Fig. 1 shows a portion of the band structure, calculated with 113 plane waves. The bottom of the conduction band at the Γ-point is taken to be E = 0, while the p-states which generate the spin-orbit interaction lie at about E_g = 13.8 eV. With the band structure, the momentum matrix element can be calculated: $P = |\langle S|p_z|Z\rangle|$, where S is the s-state at E=0, Z is the z-directed p-state at k=0, while p_z is the z-component of the momentum operator. The Rashba coefficient, α, can then be approximated as:

$$\alpha = (eP^2/3)(1/E_g^2 - 1/(E_g + \Delta_{so})^2)E_z \ ,$$

where Δ_{so} is the atomic spin-orbit energy of the 2p states (0.122 meV from optical data [6]), and E_z is the z-directed electric field in the He below the electron [7].

Another consideration is the fraction of the electron which lies in the He, where it feels the spin-orbit interaction. For simplicity we calculated this fraction by assuming the helium acts as a 1 eV abrupt barrier, and calculating the decay of the electron wave function into the barrier. The resulting factor is small, with the probability of finding the electron in the He about $3x10^{-5}$.

Combining these factors we find the Rashba effective magnetic field for an electron bound to helium is about 0.13 μG, which can be contrasted with the effective field we found experimentally for electrons at the Si/SiGe interface of about 10 G [8]. Assuming a mobility of about $5x10^6$ cm^2/Vs, and the associated motional narrowing as the electrons scatter (randomizing the direction of the Rashba effective field), we obtain a T_2 of ~ 4 months. Takeda and Kohn [4] published another set of He pseudopotentials including p- and d-wave components (optimized for He scattering from metal surfaces), but the resulting T_2 is over 10 years. In any case, we can conclude that the Rashba spin-orbit interaction has a negligible effect on the electron spin coherence. Several factors lead to the extremely small spin-orbit interaction and the Rashba effective magnetic field seen by these electrons: (1) the electrons reside almost completely in the vacuum (< 0.01% in the He); (2) with its small nuclear charge, the intrinsic atomic spin-orbit energy is extremely small in He (and that is probably in fact an overestimate for the current situation), and; (3) the nearest p-states, which lead to the spin-orbit interaction, lie quite far above the electrons states and thus the energy denominator controlling the admixture of these p-states is large.

In a more general context, an advantageous feature of the analysis of the Rashba effect for electrons on solid helium is that, in contrast to solid-solid heterostructures, the interface between

vacuum and the crystal is very well-defined. The overall potential for an electron is periodic in the plane and is well-defined normal to the plane. This should allow us to calculate the spin-orbit coupling without needing to fully calculate the band structure inside solid helium, while again using the well-established pseudopotential of helium atoms. Our preliminary results using this approach also give an exceedingly long spin relaxation time.

We find a significantly larger effect on the spin relaxation arising from the dielectric discontinuity at the helium-vacuum interface and its associated image charge, as well as the image charge in underlying metallic gates if the He film is thin enough. These effects are not usually considered in other 2D electron systems because the more conventional spin-orbit terms dominate. At a dielectric discontinuity the magnetic field of a moving electron, at the electron's position, has been shown to be simply that generated by its moving image charge as long as the motion is well below relativistic speeds and the electron is well beyond a Fermi wavelength from the metal [9]. Thus, for an electron bound to a helium film on a metal, the two important terms arise from the electron's image in the helium, and its image in the metal. The image charge in the helium is closer, but its magnitude is much less than that of the full electron seen in the metal. For He films thicker than about 45 nm, the magnetic field from the image in the helium is larger than that from the metal, and for electrons held at 50 mK and moving at the thermal velocity, the magnetic field felt by the electron is about 20 μG. Thus, it is over two orders of magnitude larger than the Rashba effective field, though still many orders of magnitude smaller than the effective field in Si. With electron scattering this field enters the relaxation rates squared, and the calculated T_2 is about 15 hours, still long enough to be essentially irrelevant for qubits.

Another source of the spin-orbit relaxation is the admixing of several levels of motion normal to the helium surface by surface capillary waves, ripplons. As a result of this admixing, the Ehrenfest theorem that prevents spin-orbit coupling due to the potential that confines electrons to the surface no longer applies. Our preliminary calculations of the spin scattering rate still give extremely small values on the order of 10^{-4} /sec.

Taken together, these results quantify and confirm our original contention that electron spin coherence is very long in this system, and other factors, such as the quantum gate fidelities, will dominate qubit errors.

The experimental measurement of 2D electron spin coherence has proven to be particularly difficult. The fundamental hurdle is transporting a sufficient number of electrons on a helium surface into the microwave resonator for Electron Spin Resonance (ESR) experiments. Mounting a filament to deposit electrons directly in the resonator is precluded by the deleterious effect of the filament and wires on the Q-factor of the resonator. Our original plan was to transport electrons along channels fabricated in Si devices through our collaboration with Sandia National Lab. However, this approach was thwarted by E' centers (oxygen vacancies [10]) in the oxide layers of the devices. These centers have an ESR line which overlaps the free electron ($g = 2$). Additionally, T_1 and T_2 of E' centers become very long at low temperatures, making it difficult to simply wait for those signals to die out. The deposited oxides serving as interlayer dielectrics in Si devices have large densities of E' centers. We developed a mechanical apparatus for depositing the electrons on a helium film outside the resonator, and then moving the sapphire

substrate with film and electrons into the resonator (all at 400 mK), but the electrons apparently leak off during the motion. The reason for the electrons leaving the surface is unclear.

As discussed in the next section, as an outgrowth of these experiments we have demonstrated the ability to stably make very high 2D electron densities on thin He films (high for a 2D electron system on He). As part of that work we have shown that we can move these electrons along a narrow line of high-resistivity NbSi. We plan to test that approach to populating the He film inside the resonator. We are also are developing the capability to measure the spin of electrons confined in quantum dots and incorporated into planar superconducting micro-resonators. In the past we have used those techniques extensively for ESR of neutral donors in Si and Ge, but the quantum dots add a complication, in that two metal layers are needed to define the dot and hold the electrons. For example, a typical quantum dot for electrons bound to He consists of a lower electrode biased positively, and an upper electrode with a small diameter hole etched through it. The top metal receives a negative bias, and thus an electron can be attracted to the hole by the underlying positive gate. We have constructed quantum dots of this design, with diameters of 100 – 300 nm, and reported on their charging characteristics at the 2023 March APS Meeting. The difficulty of incorporating these structures into micro-resonators is that the two layers are capacitively coupled, which can lead to extra resonances and microwave leakage along the line which isn't driven. We have addressed these issues by making the lower metal layer an amorphous NbSi alloy of a composition that causes it to be very resistive, while the upper layer is Nb. The characteristic impedance of this NbSi line is far from the resonator impedance (which is designed to be small for good coupling to spins), and the NbSi is connected to a photonic bandgap filter structure to attenuate any remaining microwave loss through the NbSi line. A test structure with this design is shown in Fig. 2. While the coupling is not optimal, a Q of 1700 was measured at 4.2 K. Losses in the Nb are probably limiting the Q. Importantly, large losses from the underlying NbSi quantum dot electrode are not seen. Devices of this design, with quantum dots etched into the inductor line are being readied for testing in the dilution refrigerator.

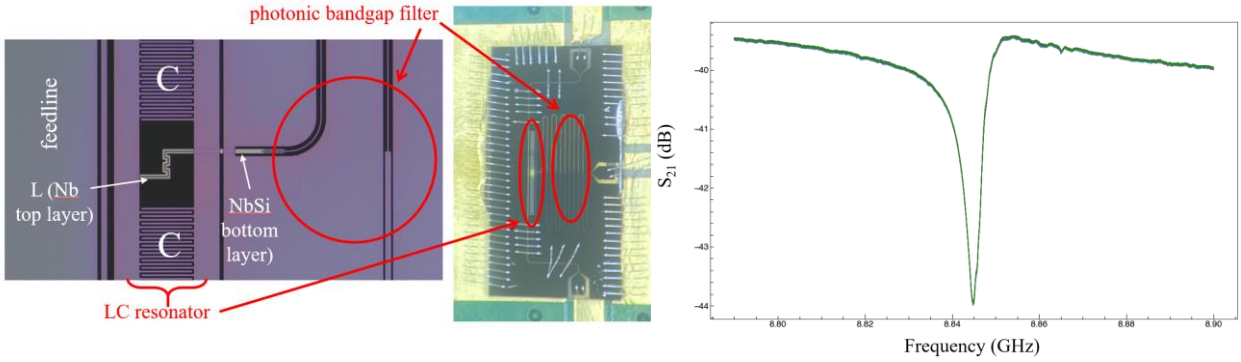

Figure 2. The left part of the figure shows the structure of the low-impedance lumped-element LC resonator, with the NbSi lower electrode leading into the photonic bandgap filter, which is most easily seen in the central photograph of the device bonded to a PC board for testing. The right side of the figure shows the transmission through the feedline, with the resonance. The coupling is not optimal, but a Q-factor of 1700 was measured at 4.2K, where losses in the Nb are significant.

High Density 2D Electron Systems

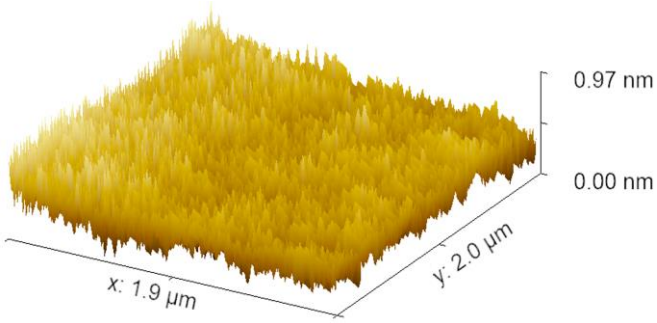

Figure 3. AFM image of an amorphous sputtered TaWSi film. The rms surface roughness over this area is measured to be 130 pm.

In developing methods to deposit high electron densities onto thin helium films we discovered new physics which is at least as interesting as the spin measurements (and may lead to a new approach for the spin experiments, as mentioned above). We have achieved electron densities sufficient to drive the electron system from a Wigner crystal to a Fermi degenerate 2D electron gas. Observation of quantum melting of the Wigner crystal has been a "Holy Grail" in this community for over 4 decades, since the first electron Wigner crystal was demonstrated with electrons on helium (Dan Tsui was looking for the analogous freezing of 2D electrons into a Wigner crystal when he found the Fractional Quantum Hall Effect).

These high-density experiments have been enabled by the amorphous metal sputtering system purchased under this grant. The key feature of the films deposited in this system is their excellent smoothness. At high electron densities the helium film is compressed to only a few nanometers, and any roughness shows up as a disorder potential for the electrons, since it modulates the distance to the electrons' image charges. In Fig. 3 we show an atomic force microscope (AFM) image of a TaWSi film.

In Fig. 4 we show a plot of the He thickness as a function of electron density, as it is compressed by the pressure from the electrons. At low densities the electrons form a classical gas. At higher densities the electrons freeze into a Wigner crystal (the red shaded region), with the density threshold set by the temperature (1.75 K, for this figure). At higher densities the Fermi energy will exceed kT, and we should expect a Fermi liquid (green shaded region). The two points at about $5x10^{11}/cm^2$ were measured using a Kelvin probe

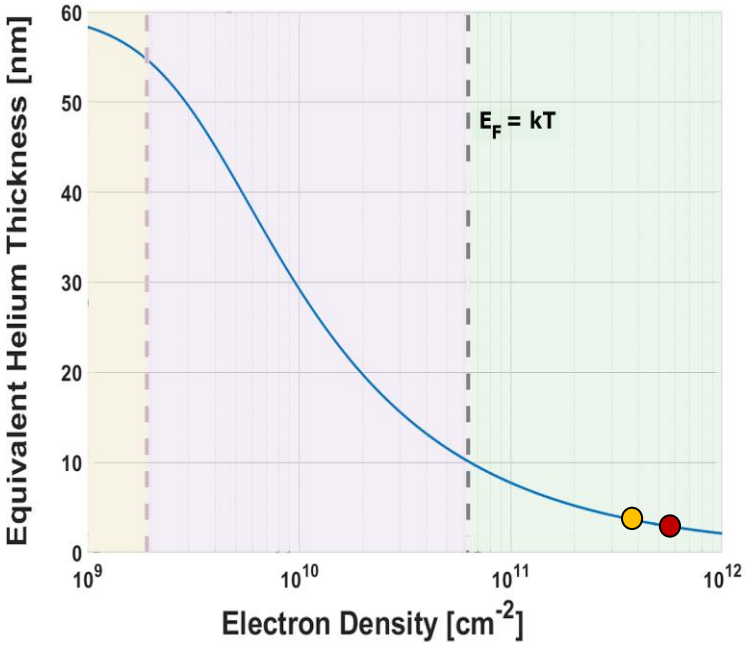

Figure 4. Plot of the effective helium thickness (includes both the helium and the distance above the He of the electron's probability density peak) as a function of electron density. The three shaded regions, left to right, are classical gas (yellow), Wigner crystal (red) and degenerate Fermi liquid (green) at 1.75 K. The two data points at $5.83 \times 10^{11}/cm^2$ and $3.75 \times 10^{11}/cm^2$ were measured with a Kelvin probe.

technique, and are from two different cool-downs. The electron density in these experiments are sufficient to put the system well into the degenerate regime. A paper describing these experiments has been published [11].

Degenerate 2D electrons bound to superfluid helium have never been conclusively demonstrated, and the transition from a Wigner crystal to a Fermi liquid has also never been definitively seen. Two factors have prevented us from declaring the observation of quantum melting of the Wigner crystal. The first is a theoretical issue; as the density increases the screening of the electron-electron interaction also increases due to the nearby metal, and the melting can be a combination of quantum effects as well as screening. Calculations of these two effects are not in full agreement [12–14]. The second factor, disorder, has been the Achilles heel of a number of other claims of quantum melting of a Wigner crystal in a variety of systems [15]. If they are strongly localized it is possible to have a high density of non-degenerate electrons.

In an as yet unpublished experiment we have shown that these high-density electrons are capable of at least slow transport. In Fig. 5 we show the device used for these experiments. It consists of two large-area amorphous NbSi films (labeled "Left" and "Right"), which have been etched to have a narrow connecting line shown in the inset. The NbSi has very high resistivity, while being extremely smooth, similar to the TaWSi shown in Fig. 3. The high resistivity of the NbSi allows us to apply different electrical biases to the left and right reservoirs, while having them connected with no gaps and no steps in the structure. Gaps or steps are large barriers for electron transport when the helium film is compressed to only a few nanometers, as shown in Fig. 4. The resistance of the narrow line is 800 kΩ, and thus negligible heating occurs, even with a 10 V bias between the two large metal areas.

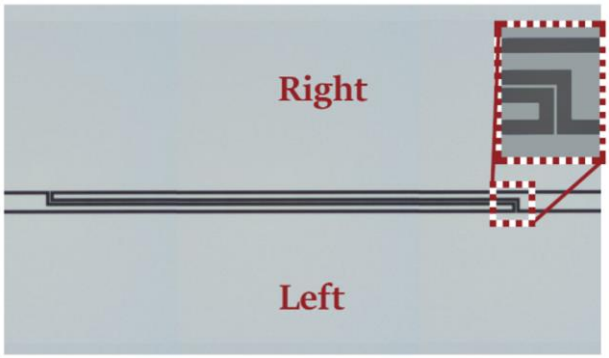

Figure 5. Photograph of a device used to measure high-density electron transport between the two large metallic areas ("reservoirs") labeled "Left" and "Right". These metal areas are sputtered amorphous NbSi alloy which is metallic but with high resistivity. The inset shows a narrow (6 μm wide) line connecting the two reservoirs.

These two reservoirs form the lower two electrodes of the Kelvin probe, while the upper electrode is split into two, allowing the measurement of the electron density above the left and right reservoirs independently. We began by charging the right reservoir, held at +2 V, to an electron density of about $2 \times 10^{11}/cm^2$, while the left reservoir was biased at -10 V to not allow any electrons to be deposited on the helium film in that region. The absence of electrons was confirmed by the Kelvin probe measurements. Next, the voltage on the left gate was made gradually more positive, and electrons were observed to transfer along the narrow line from the right to the left reservoir. Over half, but not all of the electrons could be moved to the left reservoir. These results show that at least a large fraction of the electrons are not strongly localized, but the Kelvin probe measurements are relatively slow (at least 10 s), and thus a

definitive measurement of the mobility is not possible in this manner. These results have not yet been published, but they were presented at the 2023 APS March Meeting. An additional microwave conductivity experiment is underway, which we plan to complete before publishing these results.

Electron Transport on Very Thin Helium Films

The ability to transfer electrons along the narrow NbSi line suggested another experiment to understand transport on thin helium films. There is little data on such transport for metallic films, due to the surface roughness of typical polycrystalline films and the difficulty of controlling and measuring the electrons. The transport results obtained with the device in Fig. 5 showed that the amorphous NbSi alloy layers alloy efficient electron transport. With a voltage applied to the ends of a NbSi line, electrons can be driven by a constant electric field. This opens the door to making time-of-flight mobility measurements with very thin van der Waals helium films. We have developed devices with a 3.8 mm long NbSi line (4 μm wide) that is covered by just a van der Waals film (34 nm thick in the experiments to date). At either end of this wire there is a 70 μm long transition region where the electrons are drawn up onto 0.65 μm thick helium in 10 μm wide channels. The advantage of the deeper channels is that they make it relatively straightforward to measure the electron density since narrow gaps between electrodes have little effect on the transport. We have performed time-of-flight measurements with low electron densities at 1.8 and 1.4 K. The mobility at 1.8 K was found to be about 1,700 cm^2/Vs, while at 1.4 K it rose to 16,000 cm^2/Vs. This is consistent with data on bulk helium where the mobility is governed by gas-atom scattering [16]. Importantly, these data show that the mobility on a 34 nm He film has not been degraded in that temperature range by roughness or other aspects of the metal. These are the first mobility measurements with such thin He films above a metal that we are aware of. These results were presented at the 2023 International Conference on Quantum Fluids and Solids, where the work received a Best Poster award. Some additional data is being taken, and a paper on these results is in preparation.

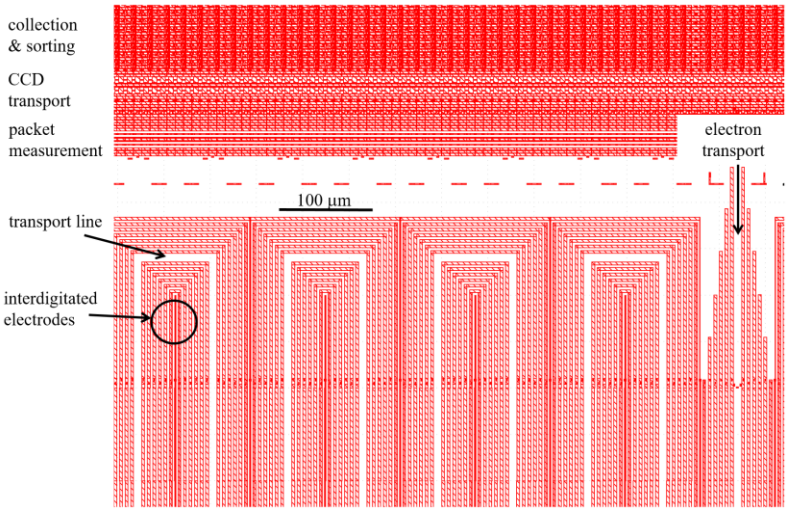

Figure 6. Image of Metal 4 (of 5 metal layers) in a device fabricated at Sandia for extending the shallow-He transport experiments to a range of He film thicknesses. Electrons are captured and sorted into small packets at the top, these electron packets can be routed with the CCD gates, measured, and launched on a NbSi transport line at the right, labeled “electron transport.” A mirror image of this structure is located at the bottom of the device (~3 mm away) , giving a total transport length of about 20 mm. The interdigitated electrodes can be used to vary the helium film thickness.

We also plan to expand on these initial experiments using devices fabricated in collaboration with our collaborators at Sandia National Lab. The ESR devices ran into the problem of interfering signals from the E' centers, but Sandia is able to fabricate an array of different devices, that fit into one field of the lithography system (reticle). We designed and Sandia has fabricated devices which will allow us to extend the range of helium film thicknesses accessible to these experiments. In Fig. 6 we show the design file for a portion of this device. This image only shows "Metal 4", the next to the top metal layer (the red hatched areas). The lower metal layers (not shown) provide all of the interconnections and wires to bring signals out to bondpads. Most of the the topmost metal layer is NbSi, deposited at Princeton. As can be seen in this image, the portion of the device fabricated at Sandia includes areas for collecting and sorting electrons into small packets, moving these electron packets to the appropriate locations with charge-coupled device (CCD) gates, and measuring the electron packets. The packets will be launched along the NbSi transport line, which is a long meander (total length about 20 mm). This figure only shows the top portion of that meandering transport line, but there is a mirror image of this structure at the bottom of the device where the electron packets will be collected, measured, and the transport timed.

A key feature of the device shown in Fig. 6 is the interdigitated electrode structure in the metal layer below the transport line. By applying a voltage between these electrodes, the thickness of the helium layer can be varied [17]. Thus, with these devices we will be able to start with a thick He film (~1 μm) , where the NbSi should have little effect on the electron mobility, but then by adjusting the voltage the film thickness can be reduced to about 20 nm. By modifying the top metal pattern of these devices, it may be possible to work with even thinner films.

Another issue which we are addressing with devices from Sandia is the difficulty of reliably detecting single electrons. The usual low-frequency capacitance techniques can be pushed down to about 10 electrons, but the best way to get better sensitivity is to incorporate the capacitance structures into a high-frequency resonator (few hundred MHz to a few GHz) [18]. A unique aspect of the fab at Sandia is their capability of using Nb as the top metal (Metal 5) layer. We

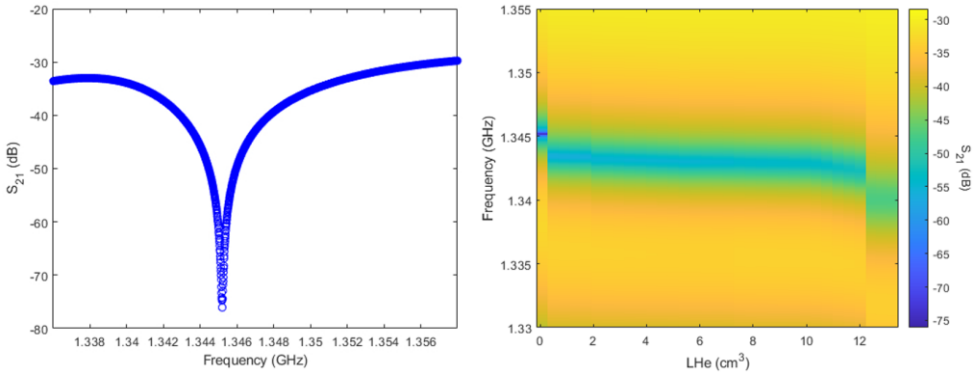

Figure 7. Measurements of a lumped-element resonant circuit in a device fabricated by collaborators at Sandia, with Nb top metal. The LC circuit is made of Nb, but a normal metal external coupling capacitor was used. The left panel shows microwave transmission at 1.8 K, with a resonance at about 1.35 GHz. The Q-factor of this circuit is about 1300. The right panel plots the color-coded transmission as a function of the amount of helium in the cell. The resonant frequency jumps down at about 0.4 cm^3 of He, and there is a large jump down in frequency at about 12 cm^3

designed superconducting LC-resonators into some of the devices they have fabricated as part of this collaboration. Achieving optimal coupling is a trial and error process, since one cannot know the losses *a priori*. We designed some structures with our best estimate of the proper coupling capacitors, but also left other areas of the Nb unpatterned, so that we can tweak the coupling.

In Fig. 7 we show measurements from a resonant structure for which we used an external capacitor to adjust the coupling, but the resonator is all Nb, to improve the Q. The Q of this structure is about 1300. Fig. 7 also shows how the resonance frequency shifts as the cell is filled with He. There is an abrupt shift down in frequency at about 0.4 cm^3 since that is when bulk He begins to accumulate in the bottom of the cell, and superfluid wicks up and fills the gaps in the interdigitated capacitor. There is another abrupt shift down in frequncy at about 12 cm^3. At this filling the helium completely submerges the resonant structure, again raising the capacitance. These data unambiguously confirm that the resonance being measured is that of the LC structure on the device, rather than a spurious resonance from other elements of the circuit. As an experimental tool, the data also give us a simple calibration to admit the correct volume of helim. With these data we know that the Nb in the Sandia process can produce good resonators, and fully on-chip structures are being designed and etched into the unpatterned Nb regions for testing the low-noise detection of single electrons. Sandia is also depositing NbN, a high kinetic inductance superconductor, on some devices which will allow for higher impedance resonators and better electric field coupling to the electrons.

References:

[1] M. I. Dykman, O. Asban, Q. Chen, D. Jin, and S. A. Lyon, *Spin Dynamics in Quantum Dots on Liquid Helium*, Phys. Rev. B **107**, 035437 (2023).

[2] C. C. Grimes, *Electrons in Surface States on Liquid Helium*, Surf Sci **73**, 379 (1978).

[3] M. V. Rama Krishna and K. B. Whaley, *Excess-Electron Surface States of Helium Clusters*, Phys. Rev. B **38**, 11839 (1988).

[4] Y. Takada and W. Kohn, *Scattering of Evanescent Waves with Application to Atom-Surface Interactions*, Phys. Rev. B **37**, 826 (1988).

[5] B. Space, D. F. Coker, Z. H. Liu, B. J. Berne, and G. Martyna, *Density Dependence of Excess Electronic Ground-State Energies in Simple Atomic Fluids*, J. Chem. Phys. **97**, 2002 (1992).

[6] J. Sansonetti, *Handbook of Basic Atomic Spectroscopic Data, NIST Standard Reference Database 108*, https://doi.org/10.18434/T4FW23.

[7] R. Winkler, *Spin-Orbit Coupling Effects in Two-Dimensional Electron and Hole Systems: With 26 Tables* (Springer, Berlin Heidelberg, 2003).

[8] A. M. Tyryshkin, S. A. Lyon, W. Jantsch, and F. Schaffler, *Spin Manipulation of Free Two-Dimensional Electrons in Si/SiGe Quantum Wells*, Phys. Rev. Lett. **94**, 126802 (2005).

[9] J. S. Shier, *Fields Due to a Slow Charged Particle Moving Parallel to a Plane-Metal Surface*, Am. J. Phys. **36**, 245 (1968).

[10] F. J. Feigl, W. B. Fowler, and Yip, Kwok L, *Oxygen Vaacancy Model for the E' Center in Si02*, Solid State Commun. **14**, 225 (1974).

[11] K. E. Castoria and S. A. Lyon, *Measurement of High Density Electrons Above a Helium Film on an Amorphous Metal Substrate*, J. Low Temp. Phys. **210**, 441 (2023).
[12] F. M. Peeters and P. M. Platzman, *Electrons on Films of Helium: A Quantum Mechanical Two-Dimensional Fermion System*, Phys. Rev. Lett. **50**, 2021 (1983).
[13] F. M. Peeters, *Two-Dimensional Wigner Crystal of Electrons on a Helium Film: Static and Dynamical Properties*, Phys. Rev. B **30**, 159 (1984).
[14] M. Saitoh, *Melting Temperature of Two-Dimensional Electron Crystals Trapped on Thin-Film Liquid He*, Phys. Rev. B **40**, 810 (1989).
[15] M. Shayegan, *Wigner Crystals in Flat Band 2D Electron Systems*, Nat. Rev. Phys. **4**, 212 (2022).
[16] M. Saitoh, *Warm Electrons on the Liquid ^{4} He Surface*, J. Phys. Soc. Jpn. **42**, 201 (1977).
[17] P. Roche, G. Deville, K. O. Keshishev, N. J. Appleyard, and F. I. B. Williams, *Low Damping of Micron Capillary Waves on Superfluid 4 He*, Phys. Rev. Lett. **75**, 3316 (1995).
[18] J. I. Colless, A. C. Mahoney, J. M. Hornibrook, A. C. Doherty, H. Lu, A. C. Gossard, and D. J. Reilly, *Dispersive Readout of a Few-Electron Double Quantum Dot with Fast Rf Gate Sensors*, Phys. Rev. Lett. **110**, 046805 (2013).

Project Information

Publications acknowledging award:

[1] K. Moskovtsev and M. I. Dykman, *Mobility of a Spatially Modulated Electron Liquid on the Helium Surface*, Phys. Rev. B **101**, 245435 (2020).

[2] A. D. Chepelianskii, D. Konstantinov, and M. I. Dykman, *Many-Electron System on Helium and Color Center Spectroscopy*, Phys. Rev. Lett. **127**, 016801 (2021).

[3] M. I. Dykman, O. Asban, Q. Chen, D. Jin, and S. A. Lyon, *Spin Dynamics in Quantum Dots on Liquid Helium*, Phys. Rev. B **107**, 035437 (2023).

[4] K. E. Castoria and S. A. Lyon, *Measurement of High Density Electrons Above a Helium Film on an Amorphous Metal Substrate*, J. Low Temp. Phys. **210**, 441 (2023).

Graduate students supported:

Kyle Castoria
Matthew Shulz
Tiffany Liu
Weiheng Fu
Gordian Fuchs
Joseph Kitzman
Camille Mikolas

Students earning PhDs

Kyle Castoria
Joseph Kitzman

Postdoctoral fellows supported:

Emil Joseph
Ofek Asban